Kramers–Kronig Receivers for 100-km Datacenter Interconnects

Xi Chen, *Member, IEEE*, Cristian Antonelli, *Member, IEEE*, Sethumadhavan Chandrasekhar, *Fellow, IEEE*, Gregory Raybon, *Fellow, IEEE*, Antonio Mecozzi, *Fellow, IEEE*, Mark Shtaif, *Fellow, IEEE*, and Peter Winzer, *Fellow, IEEE*

(Post-Deadline Paper)

***Abstract*—In this paper, we review in detail experimental demonstrations of Kramers–Kronig (KK) based direct detection systems with high per-carrier interface rates, high spectral efficiencies, and ∼100-km reach. Two realizations of KK-based receivers are summarized, including single-polarization and dual-polarization versions. Critical aspects of the KK receiver such as the carrier-to-signal power ratio and receiver bandwidth limitations are discussed. We show 220-Gb/s single-diode detection and 4 × 240-Gb/s dual polarization (dual-diode) detection in a WDM system at 5.3 bits/s/Hz spectral efficiency.**

***Index Terms*—Data center interconnect, direct detection, Kramers–Kronig receiver, short-reach transmission.**

I. Introduction

HIGH-CAPACITY data center interconnect (DCI) applications require cost-effective per-carrier interface rates beyond 100 Gb/s at a limited reach of up to ∼100 km of standard single-mode fiber (SSMF), without optical chromatic dispersion (CD) compensation due to operational simplicity and cost considerations. As the cost per fiber pair for such links can be comparable to the cost of a transponder pair, significant wavelength-division multiplexing (WDM) at high spectral efficiencies is desired for an overall lowest-cost solution. To minimize the impact of fiber dispersion, systems working near the zero-dispersion wavelength of SSMF around 1310 nm have been proposed as potential solutions [1], [2]. However, this eliminates the possibility of massive WDM, both due to the absence of adequate low-cost amplification schemes and due to the increase in CD for edge WDM channels populating higher-CD wavelengths across a reasonably wide WDM bandwidth. Within the amplification bandwidth of Erbium-doped fiber amplifiers (EDFAs) around 1550 nm, however, conventional intensity-modulation and direct detection (IM-DD) systems suffer from dispersion-induced frequency-selective power fading across the signal bandwidth [3]. For a massive WDM system occupying the full C-band, this is also true if a fixed dispersion-compensation module (DCM), e.g., a dispersion-compensating fiber, is used to compensate the CD of the transmission fiber: Even for a DCM that is nominally perfectly matched to a ∼100-km SSMF, dispersion slope mismatch and manufacturing tolerances produce enough residual CD to prevent reliable full-band system operation based on conventional IM-DD solutions. For example, a 56-GBaud 4-ary pulse amplitude modulated (PAM-4) IM-DD system carrying 100 Gb/s per wavelength at only a modest spectral efficiency of between 0.5 and 1.5 b/s/Hz may be expected to have a CD tolerance of about ± 30 ps/nm [4], which is less than the ±35 ps/nm of dispersion-slope induced CD mismatch across the C-band for a nominally perfectly compensated 100-km SSMF [5]. In general, there are several ways to avoid or to mitigate the frequency-selective power fading so as to increase the CD tolerance and altogether eliminate the need for DCMs:

- One method is to perform direct detection of only one side of the optical spectrum [6], [7], [8], which results in single side band (SSB) power detection. To fulfill the SSB condition, the other side of the spectrum must either be suppressed during modulation by means of optical field modulation (via an in-phase/quadrature (I/Q) modulator) [7], [8], or it must be rejected by an optical filter placed at the transmitter or at the receiver [6]. Using an I/Q modulator requires two digital-to-analog converters (DACs) and associated driver amplifiers and wastes half of the available modulation bandwidth. Creating SSB using optical filters requires a sharp optical filter whose center frequency is locked to the transmit laser's frequency. If the SSB filter is only used at the receiver, between 1/2 and 1/3 of the channel bandwidth is wasted.
- The second way to avoid power fading is to perform dispersion pre-compensation and to transmit the pre-distorted signal using an I/Q modulator [9], [10]. This requires

Manuscript received October 4, 2017; revised December 3, 2017 and January 8, 2018; accepted January 9, 2018. Date of publication January 29, 2018; date of current version February 24, 2018. This work was supported in part by an Institute for Information & Communications Technology Promotion grant from the Korean government (MSIP), B0101-16-0021, "Development of key technologies for flexible optical nodes in software-defined network". The work of C. Antonelli and A. Mecozzi was supported in part by the Italian Government under project INCIPICT. The work of M. Shtaif was supported in part by the Israel Science Foundation (grant 1401/16). *(Corresponding author: Xi Chen.)*

X. Chen, S. Chandrasekhar, G. Raybon, and P. Winzer are with the Nokia Bell Labs, Holmdel, NJ 07733 USA (e-mail: xi.v.chen@nokia-bell-labs.com; chandra.sethumadhavan@nokia-bell-labs.com; gregory.raybon@nokia-bell-labs.com; peter.winzer@nokia-bell-labs.com).

C. Antonelli and A. Mecozzi are with the Department of Physical and Chemical Sciences, University of L'Aquila, L'Aquila 67100, Italy (e-mail: cristian.antonelli@univaq.it; antonio.mecozzi@univaq.it).

M. Shtaif is with the Department of Physical Electronics, Tel Aviv University, Tel Aviv 69978, Israel (e-mail: shtaif@tauex.tau.ac.il).

Color versions of one or more of the figures in this paper are available online at http://ieeexplore.ieee.org.

Digital Object Identifier 10.1109/JLT.2018.2793460

advance knowledge of the transmission fiber (distance, dispersion coefficient, etc.), which essentially necessitates practically undesirable feedback mechanism from the receiver (RX) to the transmitter (TX).

- The third way to resolve power fading is to use conventional coherent receivers to detect the full optical field. Coherent receivers can either use an intradyne configuration (two balanced detectors per polarization) or a heterodyne setup (one detector of twice the bandwidth per polarization compared to intradyne). In both cases, a full coherent receiver needs a local oscillator (LO) laser, either optical polarization tracking or a polarization diversity setup, and preferably uses balanced photodetectors to suppress signal-signal beat interference (SSBI) at reasonably low LO powers. While probably the best long-term solution, its associated complexity makes a full coherent receiver currently not the most cost-efficient candidate for cost sensitive DCI applications.
- As an alternative to conventional coherent receivers, several self-coherent solutions that can detect a single-polarization optical field without an LO have been proposed [11]–[15]. Self-coherent detection uses a CW tone generated from the transmit laser that is transmitted together with the modulated signal. This enables a single-ended detector per polarization to perform coherent detection. Self-coherent detection has the benefit of eliminating the need for polarization tracking, as the LO co-propagates with the signal and therefore undergoes the same polarization rotations as the signal; hence the two stay polarization-aligned (provided that higher-order polarization mode dispersion is negligible). However, self-coherent approaches cannot make use of balanced detection and hence either require a high CW-to-signal power ratio (CSPR, defined as $\mathrm{CSPR} = \mathrm{P_{CW}}/\mathrm{P_{SIG}}$, where $\mathrm{P_{SIG}}$ contains the modulated signal only, not the CW component), leading to a loss in receiver sensitivity and hence in reach [11], or they involve iterative digital signal processing (DSP) procedures for signal-signal beat interference (SSBI) cancellation, which increase the receiver's DSP complexity [15].
- Stokes vector receivers are yet another alternative to coherent receivers [16], [17], [18], [19]. Stokes vector based systems can be configured either in a self-coherent flavor to detect the optical field [16], [17], or in a power detection arrangement to detect 3-dimentional or 4-dimentional intensity modulated signals [18], [19]. The self-coherent version of Stokes receivers can do digital dispersion compensation at the receiver, capable of transmitting signals over more than 100-km dispersion uncompensated SSMF, and ideally requires only 0-dB CSPR (meaning that the CW power is equal to the signal power). However, the receiver needs a minimum of 3 photodiodes and a minimum of 3 analog-to-digital converters (ADCs), and possibly an optical hybrid.
- Another alternative method to recover the optical field is the recently proposed Kramers-Kronig (KK) receiver [20]. The KK receiver uses a single single-ended photodetector and re-constructs the full single-polarization optical field using DSP after detection, either based on a self-coherent setup (i.e., with a CW tone added to the signal at the TX) or in a heterodyne configuration (i.e., with a CW tone added at the RX). In both configurations, the required CSPR is theoretically only ∼6 dB and in experiments typically between 7 to 9 dB, which makes the KK receiver an attractive option for low-cost, low-power, low-footprint DCI solutions that require high interface rates [15], [21], [22]. The KK receiver has been experimentally demonstrated at an interface rate of 220 Gb/s per channel [21], 256 Gb/s per channel [22], and 440 Gb/s per channel [23].

Note that the above description does not represent a mutually exclusive categorization. For instance, a Stokes receiver with signal in one polarization and CW light in the orthogonal polarization, as demonstrated in [16] can also be viewed as a self-coherent receiver. Similarly, a KK system with a CW tone transmitted together with the signal can be viewed as a self-coherent receiver. A KK receiver can also be viewed as a heterodyne receiver with single-ended detection and extra DSP.

In this paper, we (i) review the principle of KK receivers, (ii) describe our experimentally demonstrated single-photodiode based single-polarization results [21], and (iii) discuss our polarization-division multiplexed (PDM) KK receiver architecture using a local oscillator in a WDM context [24]. We compare different possible approaches to add CW light for KK detection. We review in detail our previously demonstrated transmission experiments at a line rate of 220 Gb/s (which was originally reported as 218 Gb/s, as we did not include OFDM overheads in the reported line rate [21]) at 1550 nm over 100-km SSMF using a single-polarization KK receiver with 60-GHz bandwidth. We also explain possible signal degradations for KK receivers in a WDM scenario and review our demonstrated 100-km SMF transmission in a 4-channel WDM and PDM system with 240 Gb/s per polarization-multiplexed channel using a PDM KK receiver at 24 GBaud (24.24 GHz optical bandwidth). We extend our previously published papers by describing the design details of our KK based WDM system, including a detailed account on how the lasers from the KK based transceiver can be shared between TX and RX, and how the multiplexer (Mux) and de-multiplexer (DeMux) filters can be designed in terms of frequency plan and bandwidths such that the tolerance to filter wavelength drifts is maximized. We also report on the impact of receiver frontend amplitude and phase responses on KK receivers, an important aspect that has so far been largely neglected in the KK literature. The simulation results indicate that receiver frontend electrical distortions need to be compensated *before* the waveform can be used for KK processing. We also correct a mistake contained in our previous work [21], [24], where a transmission distance of 125 km was erroneously reported. The actual transmission distance in these experiments was 100 km.

II. Minimum-Phase Signals and Kramers-Kronig Detection

The KK algorithm is a DSP procedure that is capable of reconstructing the full complex received optical field from the beating of the signal with a CW tone at the edge of the signal spectrum, as shown in Fig. 1.

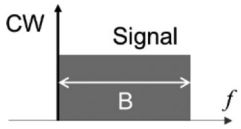

Fig. 1. Schemetic optical spectrum for KK receivers. *B* is the optical signal bandwidth.

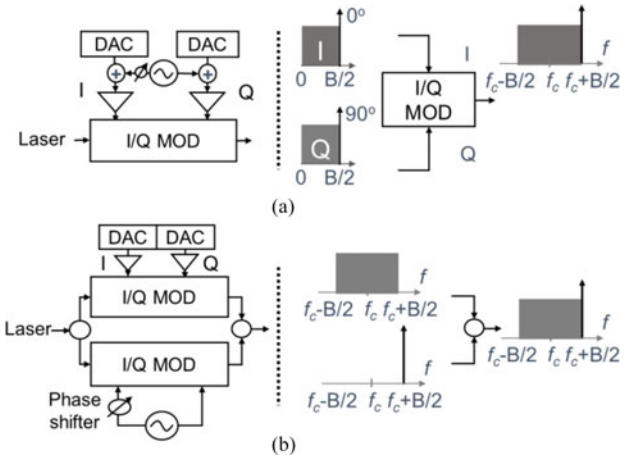

Fig. 2. Schematic diagram for different ways to add the CW tone at the transmitter for KK detection.

Importantly, this CW tone neither has to be locked in frequency nor in phase to the signal and can be generated either electronically together with the signal (as shown in Fig. 2(a), where f_c is the laser frequency), or optically through a B/2 transmit laser wavelength shifter [25], realized via an I/Q modulator and an RF synthesizer (Fig. 2(b)). The advantage of the first method is its lower optical complexity, but adding an RF tone in the analog domain to a broadband signal either induces 6 dB of RF loss or requires a sharp RF diplexer which adds analog complexity to the system. Generating and adding the tone digitally before the DACs [22] reduces the DAC resolution for the information bearing signal, thereby affecting both attainable interface rate and spectral efficiency.

The KK based optical field re-construction requires the detected optical signal to be minimum-phase [20], [27]. When this condition is satisfied, the phase information can be obtained from the magnitude spectrum via a Hilbert transform [26], [27]. In practice, for bandwidth-limited optical signals, satisfying the minimum-phase condition means that the power of the optical carrier needs to exceed a certain level [27]. Details of the KK principle can be found in [20], and the necessary and sufficient condition for minimum phase is mathematically proven in [27].

We briefly review the key algorithm making up the KK receiver DSP. We denote the complex envelope of the incoming optical field by $E_s(t)$, which is assumed to be contained within an optical bandwidth *B*, as shown in Fig. 1. The CW tone is assumed to have an amplitude E_0 and its frequency approximately coincides with the low-frequency edge of the information-carrying signal spectrum. (Placing the tone at the high-frequency edge of the signal spectrum, as shown in Fig. 2, is equally possible.) The complex envelope of the field impinging upon the photodiode is thus given by $E(t) = E_s(t) + E_0 \exp(-i\pi Bt)$.

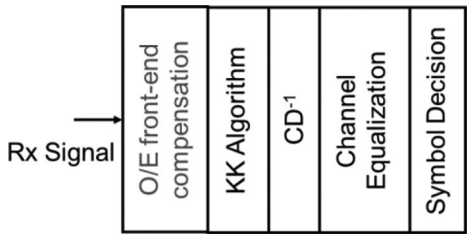

Fig. 3. DSP blocks in a single-polarization KK receiver.

The current *I(t)* produced by the photodiode is proportional to the optical intensity

$$I(t) = |E(t)|^2 = |E_s(t)|^2 + 2\mathrm{Re}\left(E_s(t)\, E_0^{\dagger} e^{i\pi Bt}\right) + |E_0(t)|^2 \tag{1}$$

where $E_0^{\dagger}$ is the conjugated field. Assuming that E_0 is large enough to ensure that the signal is minimum-phase, the following equations can be used to extract the optical field [20]:

$$E_s(t) = \left\{\sqrt{I(t)}\, \exp\left[i\phi_E(t)\right] - E_0\right\} \exp(-i\pi Bt) \tag{2}$$

$$\phi_E(t) = 1/2\pi\, p.v. \int_{-\infty}^{\infty} dt' \log[I(t')]/(t-t') \tag{3}$$

Here, *p.v.* stands for the Cauchy principal value of the integral.

The full DSP procedure is depicted in Fig. 3. After optional opto-electronic front-end correction (which is not done in our experiments but is studied in Section VII) and subsequent KK optical field re-construction, digital CD compensation can be applied. The dispersion compensated signal can then be equalized by adaptive equalizers to compensate for channel distortions, similar to what is done in a standard intradyne signal processing chain. Finally, symbol decisions can be made.

According to the theoretical derivation of the minimum-phase condition, ~6-dB CSPR is sufficient to re-construct the optical field [20], [27]. However, in practical systems, the efficiency of optical field re-construction can be reduced, e.g., by residual distortions from the receiver, as discussed in Section VII. Therefore, the required CSPR may be higher in practice, as discussed in Sections VI and VII. Depending on the overall ASE noise level and modulation format, the optimal CSPR can therefore vary. For instance, we found the required CSPR to be 7.5 dB for our 60-GHz DMT signal (220 Gb/s, bit-loaded with QPSK and 16-QAM), Section III, and as much as 9 dB for our 24-GHz dual-polarization 32-QAM (240-Gb/s) single carrier signal, Section VI.

III. Single-Polarization KK Receiver

We first constructed a single-wavelength and single-polarization system to demonstrate the KK receiver originally reported in [21].

Fig. 4 shows the experimental setup for our 220-Gb/s discrete multitone (DMT) transmission based on the KK receiver. The transmitter consists of an external cavity laser (ECL) at 1550 nm and an I/Q modulator fed by two 8-bit DACs (80 GSa/s, ~7-dB roll-off at 30 GHz) for data generation and modulation. The I/Q modulator is biased at its transmission null

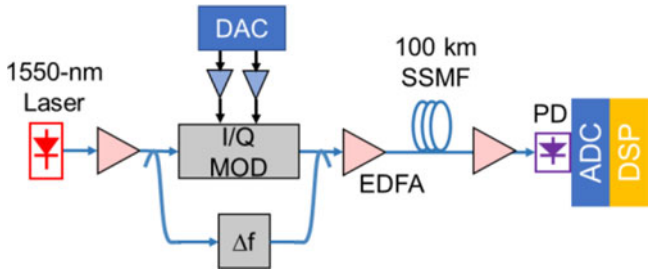

Fig. 4. Experimental setup for 220-Gb/s, single-wavelength, single-polarization, and single-photodiode KK-based direct detection system.

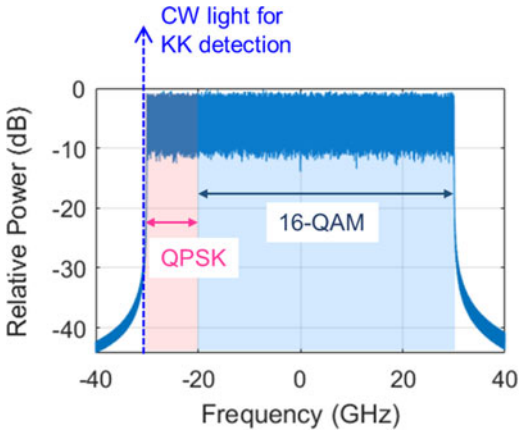

Fig. 5. Complex (I/Q) electrical spectrum at the TX for the 220-Gb/s DMT modulated signal. The blue dashed arrow indicates the position of the CW light that is later optically added to the signal for KK detection.

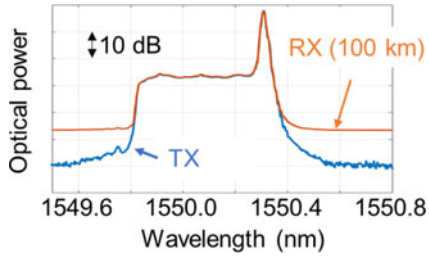

Fig. 6. Transmitted and received optical spectra of the 220-Gb/s signals.

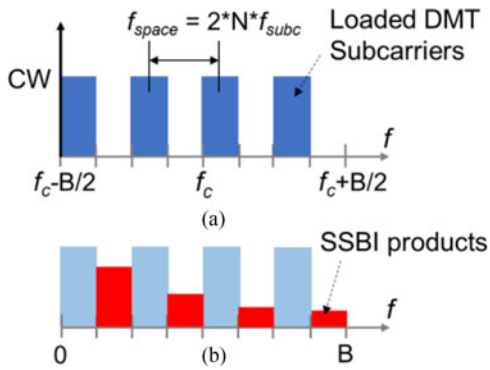

Fig. 7. Odd-index loaded DMT subcarriers (a) at the transmitter (optical) and (b) after direct detection (electrical).

and generates an optical DMT signal with 768 subcarriers. As illustrated in Fig. 5, 128 subcarriers (covering the lowest 10 GHz) are loaded with quadrature phase shift keying (QPSK), and the remaining 640 subcarriers (from 10 GHz to 60 GHz) are loaded with 16-ary quadrature amplitude modulation (16-QAM). The DC subcarrier is not loaded with data. The FFT size is 1024. Thus, the line rate (including DMT overhead) is 220 Gb/s [=(2bits∗128/1024+4 bits∗640/1024)∗80GSa/s]; without DMT overhead, we arrive at 218 Gb/s, as reported in [21]. Among the 220 Gb/s, only 0.7% overhead (8 samples) are used as guard interval. The blue arrow in Fig. 5 indicates the position of the CW light that is later optically added to the signal for KK detection.

In this experiment, we chose to generate the B/2-shifted tone *optically* (Fig. 2(b)), which saves the full DAC resolution for signal modulation and allows us to more easily vary and optimize the CSPR. In order to generate the CW tone, we split a portion of the unmodulated laser carrier and pass it through a 30-GHz sinusoidally driven $LiNbO_3$ single-sideband modulator operated as a frequency shifter (Δf) [25]. At the receiver, a single photodiode (PD, 3-dB bandwidth of 100 GHz) is used in conjunction with a single channel of a 63-GHz real-time oscilloscope acting as our ADC. Fig. 6 shows optical spectra at the TX and RX after 100 km of SSMF transmission. The received spectrum is measured after the receiver EDFA and before photo-detection. It can be observed that the noise floor is increased by more than 10 dB due to amplification, yielding a received optical signal-to-noise ratio (OSNR, 0.1 nm) of 36 dB at a total (optimum) signal launch power (including the CW tone) of 9 dBm. At the receiver, we process the sampled waveform offline and perform KK optical phase re-construction and other DSP procedures as described in Fig. 3.

Before performing actual transmission, we use a specially designed DMT signal to examine whether the KK algorithm indeed successfully re-constructs the optical field while suppressing the unwanted direct-detection SSBI, term $|E_s(t)|^2$ in (1). In particular, as shown in Fig. 7(a), we load all odd-indexed DMT subcarriers with signals and do not generate any even-indexed subcarriers. This way, all SSBI falls on even-indexed frequency bins [12] as shown in Fig. 7(b), while all desired signal-CW beat components fall on odd-indexed frequency bins, and it is therefore easy to confirm whether the KK receiver indeed successfully re-constructed the complex optical field.

The measurement results are displayed in Fig. 8, showing the recovered signal on the odd subcarriers and the residual SSBI within the even frequency slots, both with and without running the KK algorithm. The measurement is taken at a CSPR of 7.5 dB. We see that the KK algorithm reduces the SSBI by about 5 dB, as expected. We attribute the residual SSBI near DC frequencies to distortions and noise from electrical components (e.g., photodiode and scope) that affect perfect re-construction of the optical field. A more detailed discussion of this effect is given in Section VII.

We next fully load all DMT subcarriers and optimize the CSPR. Fig. 9 shows the bit error ratio (BER) averaged over all

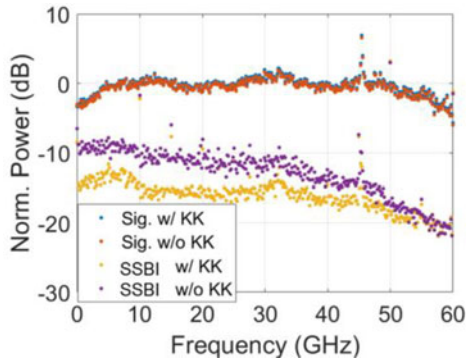

Fig. 8. Measured SSBI suppression from the KK receiver. The DC frequency corresponds to the frequency of the CW at optical domain.

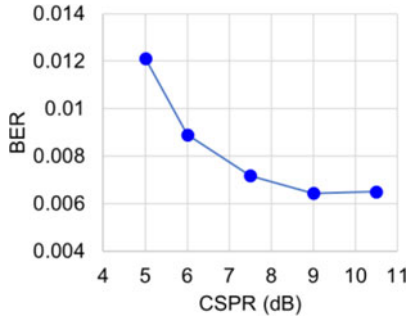

Fig. 9. BER as a function of CSPR for the 220-Gb/s signal.

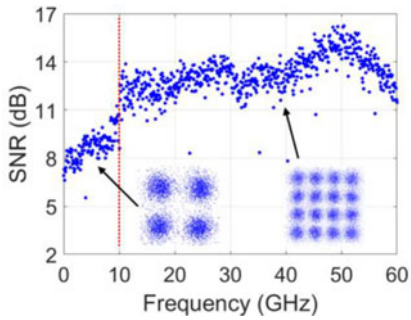

Fig. 10. SNR of the recovered constellations as a function of DMT frequencies for the 220-Gb/s signal after 100-km SSMF transmission. The DC frequency corresponds to the frequency of the CW at optical domain.

DMT subcarriers as a function of CSPR. The required CSPR to sufficiently reduce the SSBI is found to be about 7.5 dB for our single-polarization DMT signal. We use this value of CSPR for subsequent fiber transmission.

After one span of 100-km SSMF transmission, the received signal-to-noise ratios (SNRs) of the re-constructed constellations of all subcarriers are shown in Fig. 10. The recovered 16-QAM and QPSK constellations are shown as insets. The measured BER, averaged over all DMT subcarriers, is 1.76×10^{-2}, measured with 2.1 million bits. Considering a 20% overhead soft-decision forward error correction (SD-FEC), a raw BER of up to 2×10^{-2} is assumed to be correctable to yield a net data rate of 182 Gb/s. The degraded SNR between DC and 10 GHz is apparent from Fig. 8, where the SNR after

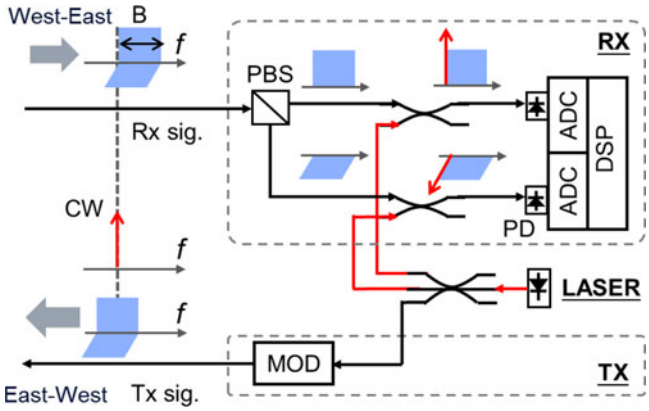

Fig. 11. Schemetic architecture of a PDM KK transceiver.

KK processing (gap between blue and orange data points) is lower in that spectral region, i.e., the residual SSBI is not removed as well there. This may be caused by magnitude and phase distortions of the opto-electronic front-end, as discussed in Section VII.

IV. Dual-Polarization KK Receiver With LO

In order to extend the KK principle to a dual-polarization scenario, a polarization-diversity setup has to be used at the receiver, as shown in Fig. 11, whereby the optical field in both polarizations is independently recovered using the KK algorithm and standard 2×2 MIMO processing is used to separate the two transmit signal polarizations. Note that in this case the CW tone can no longer be generated at the TX and transmitted together with the signal. A separate CW tone is needed at the receiver in both signal polarizations to fulfil the KK condition, but there is no passive linear optical device capable of splitting a CW light source with an arbitrary input polarization into two orthogonal polarizations with equal power [28]; therefore, a self-coherent polarization-diversity receiver architecture is not an option. For example, one might think of transmitting two identical-frequency CW tones in the two orthogonal signal polarizations, which would work if the channel was polarization maintaining. However, as these two CW tones would add up to a single tone polarized at 45 degrees (or at some elliptical superposition), it could happen for some random channel polarization rotations that the combined CW tone is aligned with one of the receiver's polarization axes. In that case, one polarization-diversity receiver path would get the full CW power while the other path would not get any CW power, which would make KK detection impossible for that second path. Counter to what is erroneously reported in [29], this problem is turned into a slow fading and is hence not resolved through different-frequency CW tones co-propagating in orthogonal signal polarizations. Therefore, if not using the Stokes vector based KK receiver as proposed in [30], the CW tone has to be generated at the RX in a polarization-diversity setup. This makes the PDM-KK setup more closely resemble a conventional heterodyne receiver. However, for conventional heterodyne detection, either the LO has

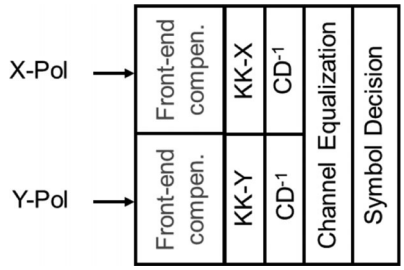

Fig. 12. DSP procedures in a polarization-multiplexed KK receiver.

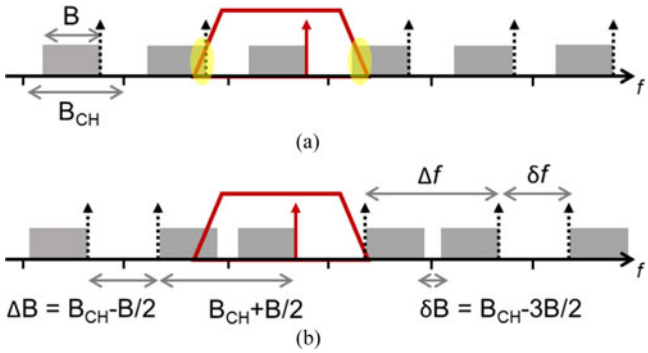

Fig. 13. Comparison of (a) convetional WDM frequency grid and (b) the proposed frequency grid.

to be chosen much stronger than the signal (for single-ended detection), or a balanced detector has to be used to suppress the SSBI component. In contrast, KK receivers need only a relatively weak LO with single-ended photodiode.

In order to save power and footprint, one may re-use a portion of the transmit laser as a CW tone for the received signal, as is done in some conventional intradyne transceivers that are not simultaneously used as regenerative wavelength converters [31]. For a KK system, this approach only works if the RX signal is shifted in frequency by B/2 relative to the TX signal, as illustrated in Fig. 11. Therefore, the lasers on one side of the link (West-East) have to be offset from the lasers on the other side of the link (East-West) by B/2. As shown in Fig. 11, the PDM received signal is first split by a polarization beam splitter (PBS). Each polarization is combined with an LO tapped from the transmit laser. The laser's wavelength and power are set to ensure the minimum-phase condition for the signal.

After detection, as shown in Fig. 12, opto-electronic front-end correction may optionally be applied (not performed in our experiments but discussed through simulation results in Section VII), and the KK algorithm is performed on each polarization separately to recover the two optical fields. Subsequently, digital dispersion compensation and standard 2x2 butterfly equalization is done to recover the PDM signals. No optical polarization tracking is needed.

Compared with the single-polarization KK setup discussed in Section III, re-using the local laser also saves energy compared to generating the tone at the transmitter, as the CW tone does not need to go through fiber transmission losses, and avoiding its electrical or optical generation at the TX significantly simplifies the TX structure. We want to re-emphasize that no phase synchronization between the CW tone and the signal is needed for the KK algorithm to work, which is particularly important when adding the CW tone at the RX instead of at the TX.

It is worth noting that we use 3-dB couplers to combine CW tone and signal in the two polarizations. This induces a 3-dB power loss on both signal and LO. However, if the system is OSNR limited, a power loss right before the photodiode does not affect performance. If system performance is limited by the receiver's electronics noise, the 3-dB loss induced by the coupler will degrade signal quality. If this is the case, 10:90 couplers can be used, emphasizing either the power-limited LO or the power-limited signal, whatever is more convenient from a system architecture perspective.

V. Bi-Directional WDM System Based on Dual-Polarization KK Receivers With LO

An important aspect of DCI WDM systems is the cost-effective implementation of optical multiplexing and demultiplexing components, notably their bandwidths, roll-offs, and frequency stabilities. As shown in Fig. 13(a), a regular WDM frequency grid (channel spacing B_{CH}) together with reasonable optical filter characteristics results in residual frequency components of the two neighboring WDM channels that would reach the photodetector of the channel to be detected. The residual signal that is further away from the CW tone (at lower optical frequencies in Fig. 13(a)) is less critical, as it produces beat signals that are out-of-band of the signal of interest. On the other hand, the residual signal that is closer to the CW tone (at higher optical frequencies in Fig. 13(a)) violates the single-sideband condition underlying the KK re-construction scheme and hence leads to worse re-construction penalties. To avoid these issues, we proposed in [24] the asymmetric WDM channel plan shown in Fig. 13(b), which ensures that the single-sideband condition is met even for realistic low-cost optical filter characteristics, without sacrificing spectral efficiency compared to Fig. 13(a). The conditions that (i) realistic WDM demultiplexers are periodic in frequency, in this case with a period of $2B_{CH}$ instead of B_{CH}, assuming an even/odd channel architecture, and that (ii) the East-West channel grid needs to be offset from the West-East channel grid by B/2 in order to re-use the TX laser as an LO, leads to the channel plan shown in Fig. 13(b), with WDM filters on a $2B_{CH}$ grid and CW tones spaced alternatingly at B_{CH}-B/2 and B_{CH}+B/2: To see this, we denote by ΔB and δB the larger and the smaller of the channel frequency gaps on an asymmetric channel grid, respectively, and write the periodicity conditions as (cf. also Figs. 14 and 15)

$$2B + \delta B + \Delta B = 2B_{Ch} \tag{4}$$

and

$$B + \Delta B = 2B + \delta B \tag{5}$$

which together yields $\Delta B = B_{Ch} - B/2$ and $\delta B = B_{Ch} - 3B/2$ for the two channel gaps, and $\delta f = B_{Ch} - B/2$, and $\Delta f = B_{Ch} + B/2$ for the large (Δf) and small (δf) laser spacings.

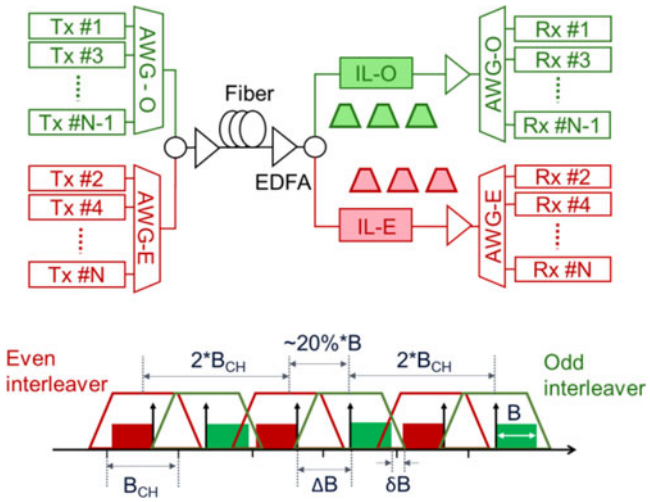

Fig. 14. WDM and PDM KK system architecture with LO. Only the West-East direction is shown. The East-West direction uses a seperate transmission fiber.

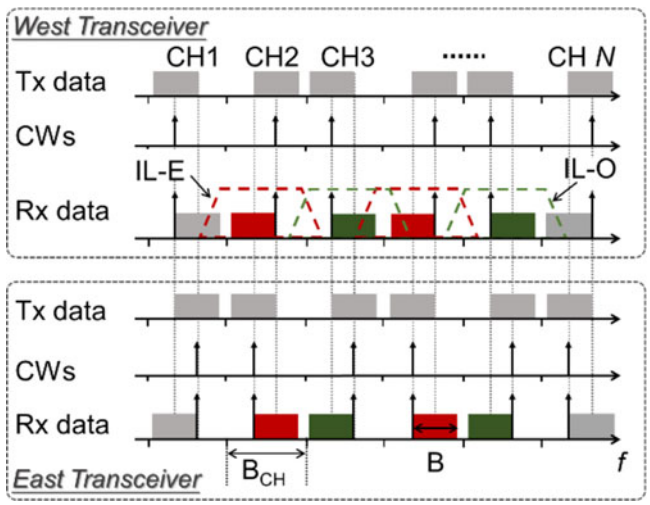

Fig. 15. Schematic spectra of the investigated WDM KK system.

To de-multiplex the WDM signals, rather than using much more difficult to fabricate narrow-band yet steep roll-off arrayed waveguide gratings (AWGs) to select individual channels, we use an interleaver (IL) based architecture in combination with AWGs at twice the bandwidth, as is commonly employed in such situations [32] and as shown in Fig. 14. The architecture is based on the fact that ILs with steep roll-offs are readily available, which significantly relaxes the roll-off and bandwidth requirements on the AWGs for cost-effective implementations. The transmit channels are combined using even and odd channel AWGs at twice the link's channel grid $\mathrm{B_{CH}}$. Even and odd channel sets are then combined using a 3-dB coupler. Optical amplifiers are used as needed to compensate for component and fiber losses. At the receiver, the WDM channels are first split by a 3-dB coupler and then filtered by two individual de-interleavers (not used to de-interleave but as periodic bandpass filters; IL-O and IL-E, for odd and even channels). The two ILs have slight frequency offsets of about $\pm 20\%$ of the signal

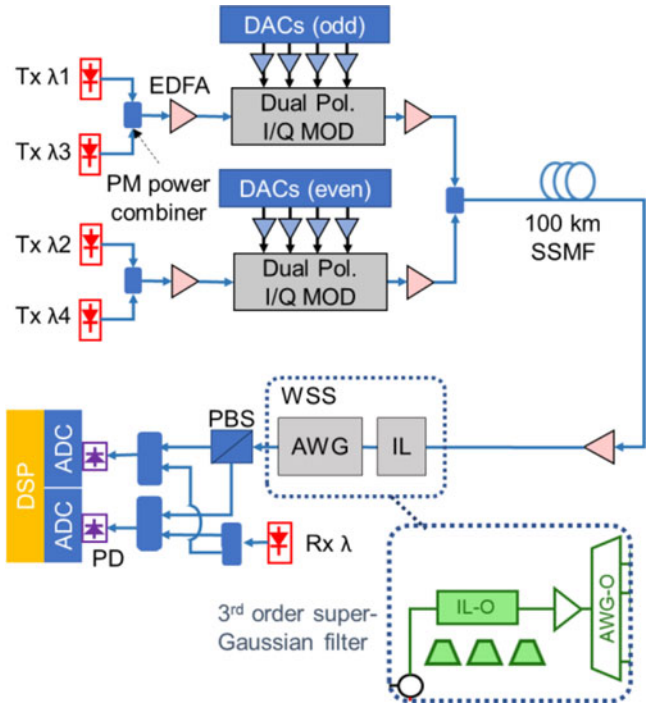

Fig. 16 Experimental setup for 4 × 240-Gb/s WDM PDM 100-km transmission based on KK receivers.

bandwidth B ($\sim\pm 5$ GHz in our case) with respect to the grid (which will become apparent in our frequency offset measurements reported in Fig. 19). Importantly, the ILs are only used as periodic filters and not to separate even and odd channels. Replacing the 3-dB splitter and the pair of ILs by a single IL could be done by foregoing the slight frequency offsets of optimally aligned IL grids. Fig. 15 sketches the overall spectral plans for TX and RX at both ends of the link. Every channel has one wide gap $\Delta \mathrm{B} = (\mathrm{B_{CH}} - \mathrm{B}/2)$ and one narrow gap $\delta \mathrm{B} = (\mathrm{B_{CH}} - 3\mathrm{B}/2)$ to its two nearest neighbors. Note that although the transponders share lasers for TX and RX in the proposed WDM architecture, the West-East and East-West links use two *separate fibers*. Therefore, interference due to bi-directional transmission is not an issue.

VI. Experimental Demonstration of WDM PDM KK

We use four channels per direction to demonstrate our proposed KK-based WDM PDM system. The experimental setup is shown in Fig. 16. At the transmitter, four ECLs around 1550 nm are used. They are grouped into odd and even channels, modulated by two dual-polarization I/Q modulators. The modulators are fed by two sets of four 8-bit DACs (88 GSa/s) for data modulation. The I/Q modulators are biased at their transmission nulls and generate two independent root-raised-cosine (RRC) shaped single-carrier 24-GBaud 32-QAM signals with a roll-off factor of 0.01. Thus, the line rate per channel is 240 Gb/s (= 5bits/symbol∗24GBaud∗2Polarizations). Odd and even channels are combined using a power combiner. In the overall channel plan, the channel grid is $\mathrm{B_{CH}} = 37.5$ GHz, the narrow frequency gap $\delta \mathrm{B} = (\mathrm{B_{CH}}\text{-}3/2\mathrm{B})$ is 1.5 GHz, and the wider fre-

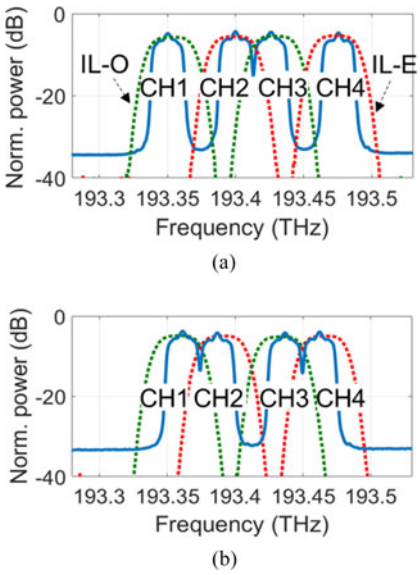

Fig. 17. Measured received optical spectra and filter shapes. (a) West-East, (b) East-West.

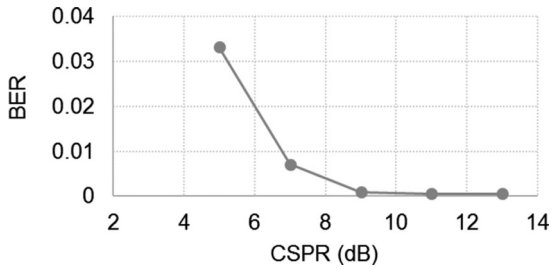

Fig. 18. BER as a function of CSPR.

quency gap $\Delta B = (B_{CH}\text{-}B/2)$ is 25.5 GHz. Considering 20% FEC overhead, the spectral efficiency of the WDM system is 5.3 bits/s/Hz (= 240 Gbps /1.2 /37.5 GHz), which is significantly higher than what can be achieved using competing single-diode approaches like IM-DD PAM-4.

After 100-km SSMF transmission, the received four channels are amplified and demutiplexed. As shown in Fig. 16, we use a wavelength selective switch (WSS) to emulate different bandwidths of the IL+AWG combination, as well as different IL center frequencies. We set the filter shape of the WSS to be a 3rd-order super Gaussian filter, which resembles a practical IL filter shape [33]. The received WDM channels and filter shapes (measured) are shown in Fig. 17. The receiver architecture and DSP follow the diagram shown in Figs. 11 and 12. The two single-ended photodiodes have a 3-dB bandwidth of 40 GHz. A 63-GHz bandwidth Keysight scope acts as a set of 2 ADCs.

We first measure the BER as a function of the CSPR in back-to-back (B2B) configuration in a single-channel scenario (when only CH3 is enabled). From Fig. 18 we see that the BER for the 240-Gb/s PDM-32-QAM signal starts to floor at ~9-dB CSPR, which is what we use for all subsequent measurements. This value is higher than the theoretically predicted ~6 dB and also slightly higher than the required CSPR (7.5 dB) for our 220-Gb/s single polarization experiment (cf. Fig. 9), but sill much less than what one would use in a typical heterodyne receiver without balanced detection.

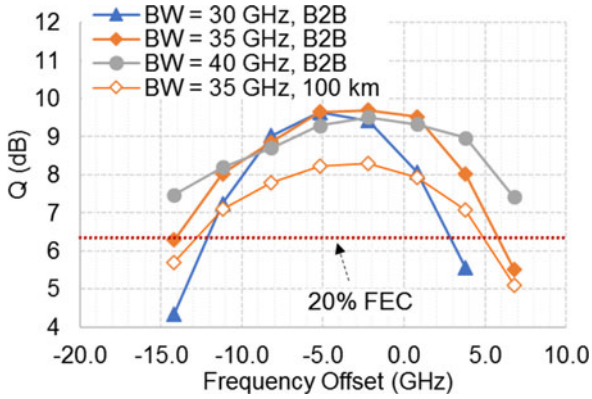

Fig. 19. BER dependence on IL filter bandwidth and frequency offset.

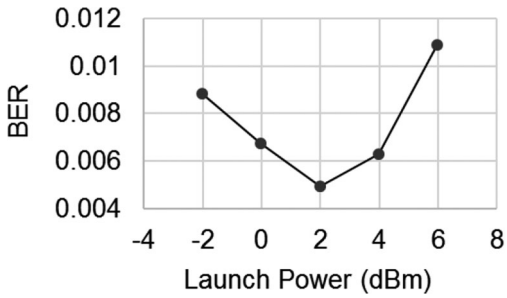

Fig. 20. BER as a function of launch power per channel.

We then study the impact of the IL characteristics (bandwidth and center frequency offset) on the WDM channels (using the middle channel CH3 as our test channel, and with all four channels enabled), with a fixed pass-band spacing of $2B_{CH} = 75$ GHz for each IL in B2B configuration. The Q factors (calculated from measured BERs) are shown in Fig. 19. It can be seen that a 35-GHz IL 3-dB bandwidth gives the best performance, with all other tested bandwidths (30 GHz and 40 GHz) also having Q factors better than the assumed 20% overhead FEC limit (BER and Q thresholds of 1.9×10^{-2} and 6.3 dB, respectively). The 35-GHz filter can drift within a 20-GHz window. Depending on the transmission distance, the tolerable drift range is slightly reduced compared to B2B. In our test case (100-km, cf. Fig. 15), the tolerable filter drift is reduced from a 20-GHz to an 18-GHz window.

The launch power is 2 dBm per channel, which was found to be optimal for the 240-Gb/s signal (cf. Fig. 20). The OSNR sensitivity for CH3 in WDM operation is shown in Fig. 21. Results are measured with a 35-GHz IL and optimal center frequencies. The required per-channel OSNR for 100-km SSMF transmission is 24 dB. About 0.8-dB penalty is observed from transmission. Insets to Fig. 21 show the constellations of the recovered PDM signal. For comparison, we also show in Fig. 21 the OSNR sensitivity of the same received signals without KK processing. It is obvious that without KK processing, the BER of the 240-Gb/s 32-QAM signal never reaches the 20% FEC threshold, even with the highest available OSNR after transmis-

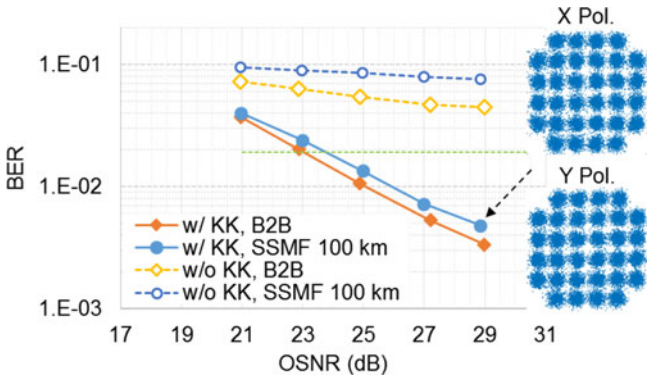

Fig. 21. OSNR sensitivity of CH3 in the described WDM scenario with (solid) and without (dashed) KK processing. Inset: recovered constellations with KK processing at an OSNR of 29 dB.

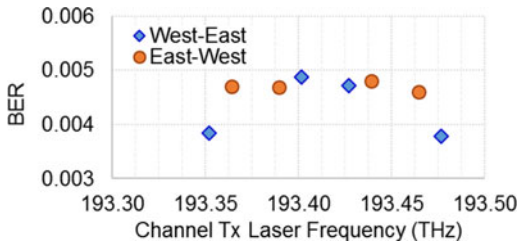

Fig. 22. 100-km SSMF transmission performance for all channels.

sion. We conclude that KK detection is a very effective way to re-construct the optical field without any iterative processing.

The BERs for all channels at full received OSNR (29 dB) are shown in Fig. 22. All BERs are well below the assumed FEC limit. CH1 and CH4 for West-East have lower BERs due to the absence of their narrow-spaced neighbors in our setup.

VII. Impact of Bandwidth Limitations on KK Receivers

In order to effectively re-construct the optical field, the KK algorithm should be fed with the squared magnitude of the optical field, without any additional distortions from the optical-to-electrical (O/E) conversion or digitization process. However, this is usually not true for a practical receiver. Typically, the receiver (photodiodes, transimpedance amplifier if used, ADCs, etc.) has bandwidth limitations as well as residual magnitude and phase responses of its constituent components. In this section, we perform numerical simulations to study the impact of receiver bandwidth limitations on the KK algorithm.

We numerically generate single-polarization data at a line rate of 128 Gb/s (a 32-GBaud 16-QAM single carrier signal with 1% RRC pulse shaping). A CW tone is added at one edge of the signal and the signal is detected by a square-law single-ended photodiode. After the photodiode, a first-order RC filter (examples shown in Fig. 23) is added to emulate magnitude and phase response of a simple opto-electronic front-end. The CSPR is kept at 8 dB for all simulations. The simulation is done in a back-to-back setting without adding chromatic dispersion. We compare the results with perfectly balanced heterodyne detection (i.e., with perfect optical field re-construction free of SSBI). The same RC filters are used for both the heterodyne receiver

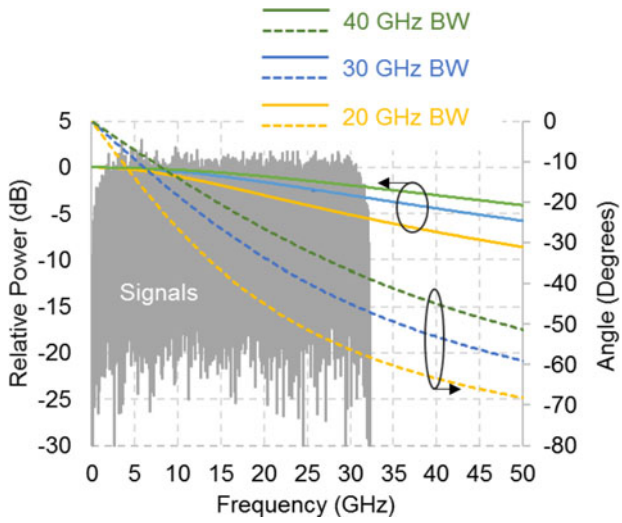

Fig. 23. Two examples of simulated bandwidth limitations of the receiver. Solid blue and yellow lines represent power profiles of the RC filters. Dashed bue and yellow lines represent phase profiles of the RF filters.

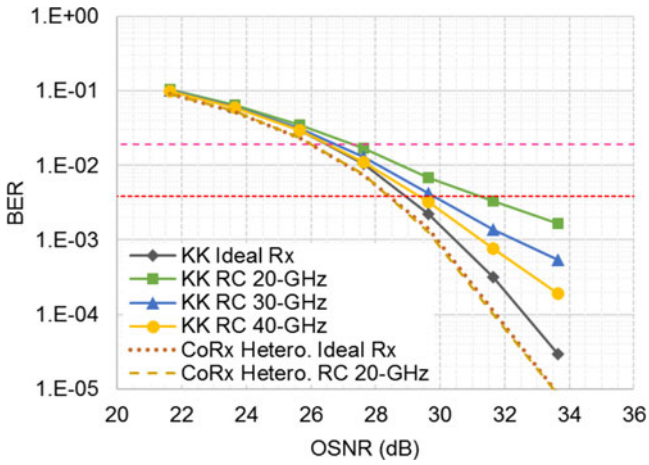

Fig. 24. OSNR sensitivity for 32-Gbaud 16-QAM KK receivers with different receiver bandwidths.

and the KK receiver. We assume that system noise is dominated by ASE, thus no receiver electronics noise is considered. This implies that the receiver only adds magnitude and phase distortions to the electrical signal, but no additional noise. After optical field re-construction, the heterodyne receiver and the KK receiver use the same DSP (a least mean square equalizer) for channel equalization. The OSNR is defined as the signal power plus the CW power divided by the noise power in two polarizations in a 0.1 nm optical noise reference bandwidth. No optical filter is used to reject the ASE noise on the other side of the CW. The simulated system setup is the same as the one shown in Fig. 4, and a perfect transmitter is assumed. This is to keep the simulation conditions as simple as possible to study only the sensitivity of KK field re-construction to electrical distortions.

We first vary the 3-dB bandwidth of the RC filter from 20-GHz to 40-GHz and check the OSNR sensitivity of the 128 Gb/s 16-QAM signal. The results are shown in Fig. 24. For comparison, we plot the OSNR sensitivity of an ideal KK receiver without bandwidth limitations for comparison. Note that due to

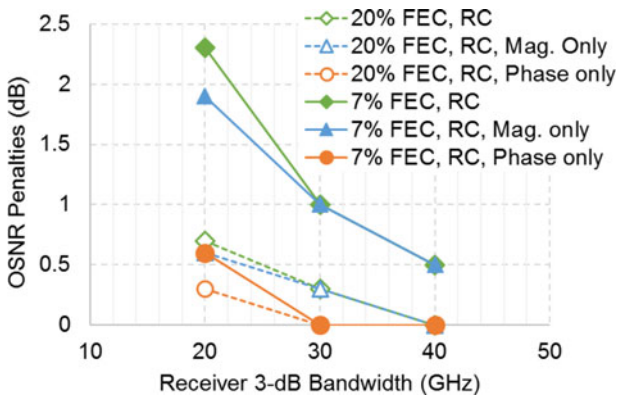

Fig. 25. OSNR penalties with phase and/or magnitude response of receivers.

the peaky nature of the 1% RRC shaped waveform, with a CSPR of 8 dB, the minimum-phase condition for KK processing is not perfectly satisfied. Therefore, the OSNR sensitivity of an ideal KK receiver is a bit worse than a balanced detector based heterodyne coherent receiver (0.5 dB worse at BER of 1×10^{-3}). Similar OSNR sensitivity differences are also observed in other simulation results [20]. It can be seen that a receiver with a 3-dB bandwidth of 20 GHz induces a 2.3-dB OSNR penalty at the 7% FEC threshold of $\mathrm{BER} = 3.8 \times 10^{-3}$. We also plot the results for an ideal heterodyne receiver, and for a heterodyne receiver with a 20-GHz RC bandwidth for comparison. As neither receiver noise nor ADC quantization are considered, the heterodyne receiver does not have any OSNR penalty for significant RC filtering, since the adaptive equalizer can always equalize the waveform. However, for KK receivers, as expected, electrical distortions affect the optical field re-construction.

We further study the impact of phase and magnitude distortions *separately*, by adding only the RC phase response or the RC magnitude response individually to the detected signals. (Conceptual concerns of violated filter causality for these hypothetic test cases can be addressed through the assumption of an additional, arbitrarily long delay element that does not affect system performance.) We simulate BER vs. OSNR curves as shown in Fig. 24 and read OSNR penalties at 20% and 7% FEC levels ($\mathrm{BER} = 1.9 \times 10^{-2}$ and $\mathrm{BER} = 3.8 \times 10^{-3}$). The penalties are shown in Fig. 25. It can be seen that the magnitude response has a much more severe impact than the phase response, but even a phase response as benign as that of an RC low-pass filter can produce a ∼0.5-dB penalty during KK detection. More abrupt phase or amplitude changes (such as those due to resonances in real high-speed electronic and optoelectronic packages) may yield more severe penalties, whose detailed study is beyond the scope of this paper.

The above simulation results indicate that magnitude and phase distortions within the signal bandwidth should be first compensated before applying the KK algorithm to re-construct the optical field effectively. While no such compensation was done in any of the experiments reported in this paper, we expect further improvement from performing the required calibration and compensation.

VIII. Conclusions

We reviewed two recently reported experimental demonstrations of KK-based receivers [21], [24], a single-diode, single-polarization KK receiver and a dual-polarization KK receiver using a local oscillator. Using a 63-GHz bandwidth single-diode KK receiver, we transmitted DMT signals with a line rate of 220-Gb/s (a net data rate of 182 Gb/s) over a 100-km SSMF link without optical dispersion management. We also demonstrated 4-channel PDM and WDM 100-km SSMF transmission based on PDM-KK receivers. The 24-GBaud 32-QAM channels were asymmetrically placed on a 37.5-GHz channel grid and the achieved spectral efficiency was 5.3 bits/s/Hz. The designed WDM system can use a practical 3rd-order super Gaussian IL shape and shows a tolerance to center frequency drifts within an 18-GHz window.

References

[1] W. Yan *et al.*, "100 Gb/s Optical IM-DD transmission with 10G-class devices enabled by 65 GSamples/s CMOS DAC Core," in *Proc. Opt. Fiber Commun. Conf. Expo. Nat. Fiber Opt. Eng. Conf.*, 2013, Paper OM3H.1.

[2] M. Chagnon *et al.*, "Experimental study of 112 Gb/s short reach transmission employing PAM formats and SiP intensity modulator at 1.3 μm," *Opt. Express*, vol. 22, pp. 21018–21036, 2014.

[3] C. Xie *et al.*, "Single-VCSEL 100-Gb/s short-reach system using discrete multi-tone modulation and direct detection," in *Proc. Opt. Fiber Commun. Conf. Exhib.*, 2015, pp. 1–3.

[4] N. Eiselt *et al.*, "First real-time 400G PAM-4 demonstration for inter-data center transmission over 100 km of SSMF at 1550 nm," in *Proc. Opt. Fiber Commun. Conf. Exhib.*, 2016, Paper W1K.5.

[5] 2017. [Online]. Available: http://fiber-optic-catalog.ofsoptics.com/Asset/OFS_SMFDK_S.pdf

[6] Q. Zhang *et al.*, "C-band 56 Gbps transmission over 80-km single mode fiber without chromatic dispersion compensation by using intensity-modulation direct-detection," in *Proc. Eur. Conf. Opt. Commun.*, 2014, pp. 1–3.

[7] L. Zhang, E. Zhou, Q. Zhang, X. Xu, G. N. Liu, and T. Zuo, "C-band single wavelength 100-Gb/s IM-DD transmission over 80-km SMF without CD compensation using SSB-DMT," in *Proc. Opt. Fiber Commun. Conf.*, 2015, Paper Th4A.2.

[8] S. Randel *et al.*, "100-Gb/s discrete-multitone transmission over 80-km SSMF using single-sideband modulation with novel interference-cancellation scheme," in *Proc. Eur. Conf. Opt. Commun.*, 2015, pp. 1–3.

[9] J. McNicol, M. O'Sullivan, K. Roberts, A. Comeau, D. McGhan, and L. Strawczynski, "Electrical domain compensation of optical dispersion," in *Proc. Opt. Fiber Commun. Conf.*, 2005, Paper OThJ3.

[10] R. I. Killey, P. M. Watts, M. Glick, and P. Bayvel, "Electronic dispersion compensation by signal predistortion," in *Proc. Opt. Fiber Commun. Conf., Nat. Fiber Opt. Eng. Conf.*, 2006, Paper OWB3.

[11] X. Chen *et al.*, "High-speed fading-free direct detection for double-sideband OFDM signal via block-wise phase switching," in *Proc. Opt. Fiber Commun. Conf., Nat. Fiber Opt. Eng. Conf.*, 2013, Paper PDP5B.7.

[12] W. R. Peng *et al.*, "Experimental demonstration of a coherently modulated and directly detected optical OFDM system using an RF-tone insertion," *Proc. Opt. Fiber Commun. Conf., Nat. Fiber Opt. Eng. Conf.*, 2008, Paper OMU2.

[13] X. Chen *et al.*, "Signal-carrier interleaved optical OFDM for direct detection optical communication," *Opt. Express*, vol. 21, pp. 32501–32507, 2013.

[14] T. Miyazaki and F. Kubota, "PSK self-homodyne detection using a pilot carrier for multibit/symbol transmission with inverse-RZ signal," *IEEE Photon. Technol. Lett.*, vol. 17, no. 6, pp. 1334–1336, 2005.

[15] Z. Li *et al.*, "Signal-signal beat interference cancellation in spectrally-efficient WDM direct-detection Nyquist-pulse-shaped 16-QAM subcarrier modulation," *Opt. Express*, vol. 23, pp. 23694–23709, 2015.

[16] D. Che *et al.*, "Stokes vector direct detection for linear complex optical channels," *J. Lightw. Technol.*, vol. 33, no. 3, pp. 678–684, Feb. 2015.

[17] M. Y. S. Sowailem *et al.*, "100G and 200G single carrier transmission over 2880 and 320 km using an InP IQ modulator and Stokes vector receiver," *Opt. Exp.*, vol. 24, no. 26, pp. 30485–30493, 2016.
[18] M. Morsy-Osman *et al.*, "Four-dimensional modulation and Stokes direct detection of polarization division multiplexed intensities, inter polarization phase and inter polarization differential phase," *J. Lightw. Technol.*, vol. 34, no. 7, pp. 1585–1592, Apr. 2016.
[19] M. Chagnon, and D. V. Plant, "504 and 462 Gb/s direct detect transceiver for single carrier short-reach data center applications." in *Proc. Opt. Fiber Commun. Conf. Exhib.*, 2017, Paper W3B.2.
[20] A. Mecozzi *et al.*, "Kramers–Kronig coherent receiver," *Optica*, vol. 3, pp. 1218–1227, 2016.
[21] X. Chen *et al.*, "218-Gb/s single-wavelength, single-polarization, single-photodiode transmission over 125-km of standard singlemode fiber using Kramers–Kronig detection," in *Proc. Opt. Fiber Commun. Conf.*, 2017, Paper Th5B.6.
[22] S. T. Le *et al.*, "8x256Gbps virtual-carrier assisted WDM direct-detection transmission over a single span of 200km," in *Proc. Eur. Conf. Opt. Commun.*, 2017, Paper Th.PDP.B.1.
[23] X. Chen *et al.*, "Single-wavelength, single-polarization, single-photodiode Kramers–Kronig detection of 440-Gb/s entropy-loaded discrete multitone modulation transmitted over 100-km SSMF," in *Proc. IEEE Photon. Conf.*, 2017, Paper Th5B.6.
[24] X. Chen *et al.*, "4 x 240 Gb/s Dense WDM and PDM Kramers–Kronig detection with 125-km SSMF transmission," in *Proc. Eur. Conf. Opt. Commun.*, 2017, Paper W.2.D.4.
[25] S. Shimotsu *et al.*, "Wideband frequency conversion with LiNbO3 optical single-sideband modulator," in *Proc. Opt. Fiber Commun. Conf.*, 2011, Paper WK-3.
[26] L. Taylor, "The phase retrieval problem," *IEEE Trans. Antennas Propag.*, vol. 29, no. 2, pp. 386–391, Mar. 1981.
[27] A. Mecozzi, "A necessary and sufficient condition for minimum phase and implications for phase retrieval," *IEEE Trans. Inf. Theory*, vol. 13, no. 9, Sep. 2016, Art. no. 04861.
[28] W. Shieh, H. Khodakarami, and D. Che, "Invited article: Polarization diversity and modulation for high-speed optical communications: Architectures and capacity," *APL Photon.*, vol. 1, 2016, Art. no. 040801.
[29] C. Wei, W. Zeng, and C. Lin, "Spectrally efficient polarization multiplexed direct-detection OFDM system without frequency gap," *Opt. Express*, vol. 24, p. 1823, 2016.
[30] C. Antonelli, A. Mecozzi, M. Shtaif, X. Chen, S. Chandrasekhar, and P. J. Winzer, "Polarization multiplexing with the Kramers–Kronig receiver," *J. Lightw. Technol.*, vol. 35, no. 24, pp. 5418–5424, Dec. 2017.
[31] L. Chen *et al.*, "Silicon photonics for coherent transmission," in *Proc. Opt. Fiber Commun. Conf.*, 2016, Paper Th1B-1.
[32] A. Gnauck *et al.*, "25 x 40-Gb/s copolarized DPSK transmission over 12 x 100-km NZDF with 50-GHz channel spacing," *IEEE Photon. Technol. Lett.*, vol. 15, no. 3, pp. 467–469, Mar. 2003.
[33] Typical spectral profiles of interleavers, 2017. [Online]. Available: http://www.optoplex.com/download/Optoplex%20Optical%20Interleaver%20Brochure%20Rev1.3.pdf

Authors' biographies not available at the time of publication.